RSCPublishing Faraday Discussions

Introductory Lecture
Supported Cluster Catalysts Synthesized to be Small,
Simple, Selective, and Stable

Journal:	*Faraday Discussions*
Manuscript ID	FD-ART-04-2018-000076
Article Type:	Paper
Date Submitted by the Author:	14-Apr-2018
Complete List of Authors:	Guan, Erjia; University of California, Department of Materials Science and Engineering Fang, Chia-Yu; University of California, Department of Materials Science and Engineering Yang, Dong; University of California, Department of Chemical Engineering Wang, Liang; Zhejiang University, Chemistry Xiao, Fengshou; Department of Chemistry, Zhejiang University Gates, Bruce; University of California, Department of Chemical Engineering

SCHOLARONE™
Manuscripts

Journal Name

ARTICLE

Supported Cluster Catalysts Synthesized to be Small, Simple, Selective, and Stable

Erjia Guan, [a,b†] Chia-Yu Fang, [a,b†] Dong Yang, [a†] Liang Wang, [c] Feng-Shou Xiao,[c] and Bruce C. Gates [a*]

Molecular metal complexes on supports have drawn wide attention as catalysts offering new properties and opportunities for precise synthesis to make uniform catalytic species that can be understood in depth. Here we highlight advances in research with catalysts that are a step more complex than those incorporating single, isolated metal atoms on supports. These more complex catalysts consist of supported noble metal clusters and supported metal oxide clusters, with emphasis placed on some of the simplest and best-defined of these catalysts, made by precise synthesis, usually with organometallic precursors. Characterization of these catalysts by spectroscopic, microscopic, and theoretical methods is leading to rapid progress in fundamental understanding of catalyst structure and function and to expansion of this class of materials. The simplest supported metal clusters incorporate two metal atoms each—they are pair-site catalysts. These and clusters containing several metal atoms have reactivities determined by the metal nuclearity, the ligands on the metal, and the supports, which themselves are ligands. Metal oxide clusters are included in the discussion, with Zr_6O_8 clusters that are nodes in metal-organic frameworks being among those understood the best. The surface and catalytic chemistry of these metal oxide clusters are distinct from those of bulk zirconia. A challenge in using any supported cluster catalysts is associated with their possible sintering, and recent research shows how metal nanoparticles can be encapsulated in sheaths with well-defined structures—zeolites—that make them highly resistant to sintering.

Introduction

Many practical catalysts consist of active species dispersed on porous supports. Common supported species are metals, metal oxides, and metal sulfides, and common supports are metal oxides, zeolites, and carbon. The supported species range in size from single metal atoms to few-atom clusters to nanoparticles. It would be an exaggeration to refer to the preparation of most supported catalysts with the term "synthesis." Rather, most are prepared by empirical routes that are complex, multistep, and economical on a large scale (e.g., impregnation of a metal oxide support with a metal salt, calcination, and reduction). It would also be an exaggeration to refer to most supported catalysts as single species. Instead, most are highly heterogeneous in composition and structure.

Our principal focus is on supported catalysts that have well-defined structures—and for which the term "synthesis" is justified. This focus points us to small, well-defined supported species that are essentially molecular in character. Thus, we minimize consideration of the large class of catalysts that consist of smears of nonuniform nanoparticles on supports, notwithstanding their great practical importance and the extensive innovative work that has led to new compositions (e.g., of bimetallics), new catalytic properties, and fundamental understanding emerging from characterization and modelling to account for both the ligands on the supported nanoparticles and the metal-support bonding.

We consider supported catalysts that are a step or two more complex than the simplest and best-defined supported catalysts—site-isolated single-metal-atom complexes (a topic that has been extensively reviewed and assessed recently[1, 2]). Thus, our primary topic is supported metal clusters, including the simplest, which consist of pairs of metal sites on supports, and those consisting of several metal atoms each. We also consider a separate class of supported clusters, metal oxides, which are synthesized to have a high degree of uniformity by incorporation in metal organic frameworks. We extend the assessment to materials synthesized to encapsulate metal nanoparticles in zeolite supports in ways that make them highly stable and resistant to sintering.

Transition of Catalytic Properties as Atomically Dispersed Supported Metal Catalysts undergo the First Steps of Metal Aggregation

Atomically dispersed supported metals are regarded as the simplest supported metal catalysts, being both a limiting case in terms of structure and a starting point for preparation of more complex supported catalysts. The metals in these most highly dispersed catalysts, in contrast to the zerovalent metals in supported metal nanoparticles, are typically positively charged. Cations of noble

[a.] Department of Chemical Engineering, University of California, Davis, California 95616, United States. E-mail: bcgates@ucdavis.edu (B.C.G.).
[b.] Department of Materials Science and Engineering, University of California, Davis, California 95616, United States
[c.] Key Laboratory of Applied Chemistry of Zhejiang Province, Department of Chemistry, Zhejiang University, Hangzhou 310028, China.
[d.] † These authors contributed equally to the paper.

metals on supports, when exposed to reducing environments, are readily reduced and aggregated to form nanoparticles. The first steps of reduction/aggregation lead to the smallest metal clusters, which may have catalytic properties markedly different from those of the single-metal-atom species and also of the nanoparticles that result from further aggregation.

For example, when atomically dispersed cationic gold complexes on CeO_2 were used in a flow reactor to catalyze CO oxidation at 353 K, the gold quickly underwent reduction and aggregation, as monitored with X-ray absorption spectroscopy of the functioning catalyst (Figure 1).[3] The catalytic activity (indicated by the CO conversion) increased markedly upon formation of even the smallest gold clusters (as indicated by extended X-ray absorption fine structure

(EXAFS) spectra determining the average Au–Au coordination number, Figure 1). During this process, the gold was reduced, as indicated by the fluorescence X-ray absorption near edge structure (XANES) data shown in Figure 1. The spectroscopic data are limited because they give only average structural information, but they provide a clear demonstration of opportunities for tailoring catalytic properties by adjusting the nuclearities of extremely small metal species. These results are reinforced by observations of catalytic reactions in solutions of AuCl, in which the ester-assisted hydration of alkynes began only when clusters of three to five gold atoms formed from the AuCl.[4] We posit that when clusters of gold and other metals are made precisely in the form of dimers, trimers, etc., they will be found to offer new catalytic properties.
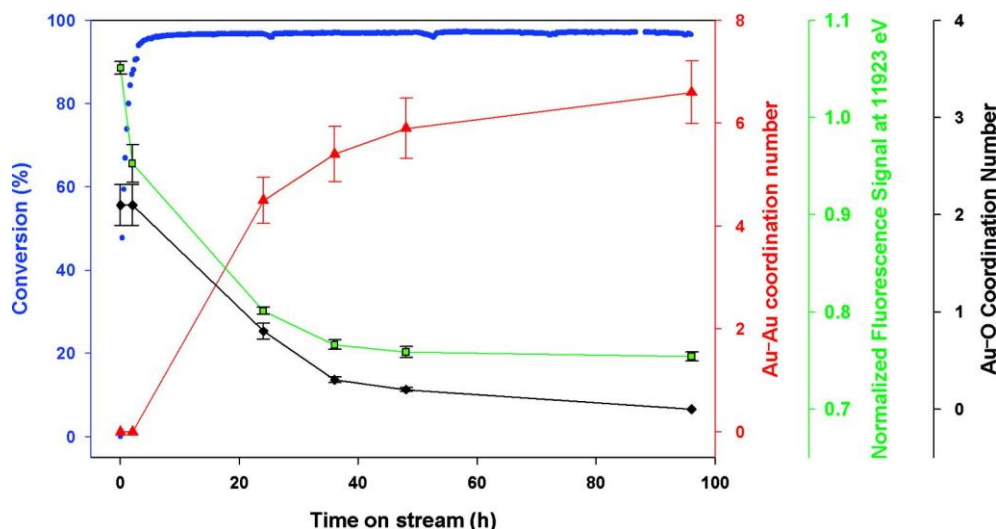

Figure 1. Catalytic activity of gold supported on CeO_2 for CO oxidation in a flow reactor at 353 K, starting with $Au(CH_3)_2(acac)/CeO_2$, $P_{CO} = 1.0$, $P_{O2} = 0.5$ kPa, which itself had a low but measurable catalytic activity. Conversion of CO (●); Au–Au coordination number, showing formation of gold clusters (▲); normalized fluorescence signal at 11923 eV, indicating the content of gold with oxidation state +3 (■); Au–O coordination number, indicating breaking of Au–support oxygen bonds as Au–Au bonds form (◆). Reproduced with permission from *J. Phys. Chem. C,* **2009***, 113,* 3259-3269. Copyright (2009) American Chemical Society.

Only little work has been reported that illustrates details of cluster synthesis on supports. For example, three-atom bimetallic clusters on high-area MgO powder were synthesized from adsorbed precursors, $Ru_3(CO)_{12}$ and $Os_3(CO)_{12}$ (the latter was converted to $[Os_3(CO)_{11}]^{2-}$ upon adsorption).[5] These monometallic clusters were initially well-separated on the support surface, as demonstrated by infrared (IR) and EXAFS spectra characterizing the isolated molecular species. When the sample was exposed to flowing H_2 as the temperature was raised, IR spectra showed that the intensity of the v_{CO} bands of $Ru_3(CO)_{12}$ began to decrease at 333 K. As the temperature was increased to 358 K, removal of CO ligands bonded to $[Os_3(CO)_{11}]^{2-}$ was also observed. Then new v_{CO} bands appeared indicating a new surface species, the bimetallic cluster $H_2Os_3Ru(CO)_{13}$, and the v_{CO} band intensity of this cluster increased and attained a maximum at 423 K. EXAFS data recorded during this synthesis (Figure 2) confirm the IR evidence of decarbonylation of $Ru_3(CO)_{12}$ and $[Os_3(CO)_{11}]^{2-}$ and also provide evidence that the ruthenium clusters began to aggregate (with the Ru–Ru coordination number increasing from the initial value of nearly 2 (1.9) to 4.0), accompanied by removal of CO ligands, while the triosmium cluster frame

remained intact during its partial decarbonylation. But as the temperature increased to 423 K, the EXAFS Ru–Ru contribution started to decrease (from 4.0 to 1.0) as ruthenium clusters broke up, and a Ru–Os contribution and an Os–Ru contribution appeared and grew, demonstrating the formation of bimetallic clusters and confirming the IR data. The loss of CO ligands from the original clusters evidently triggered the reactions leading to Ru–Os bond formation and generation of the bimetallic clusters. The steps in the synthesis of these clusters are represented schematically in Figure 3. This experimental evidence of the roles of molecular intermediates in the synthesis of a supported molecular cluster seems to be unique; it was possible to elucidate these details because two separate metals were involved and X-ray absorption spectra could be measured at each metal edge to allow identification of the bimetallic clusters.
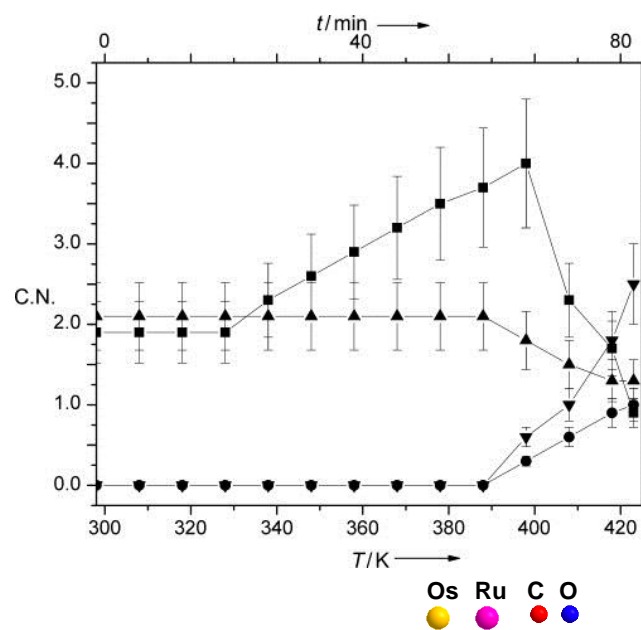
Figure 2. EXAFS data characterizing changes in coordination numbers (C.N.) of the monometallic and bimetallic species on MgO in flowing H_2 as the temperature increased from 298 to 423 K (at 1.5 K min 1) at 1 bar. ■ Ru–Ru, ● Ru–Os, ▲ Os–Os, ▼ Os–Ru. Reproduced from Reproduced with permission from *Angew. Chem. Int. Ed.* **2009**, *48*, 9697-9700. Copyright (2009) Wiley-VCH.
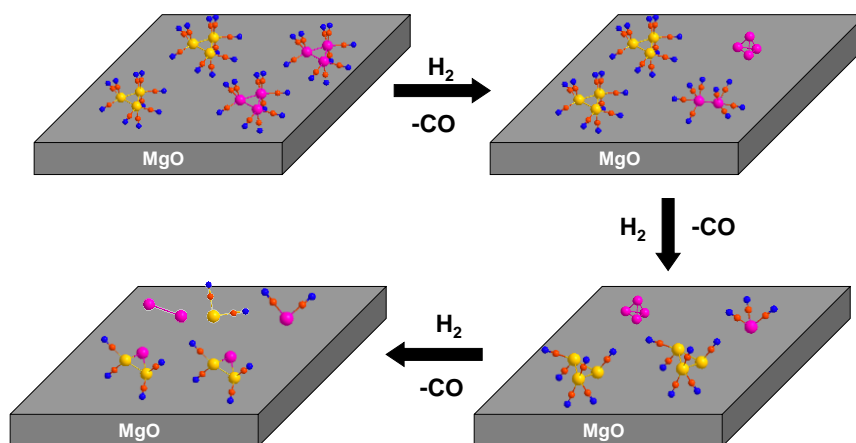

Figure 3. Model of bimetallic cluster formation in H_2 as the temperature increased from 298 to 423 at 1.5 K min^{-1}. Structural models were constructed on the basis of EXAFS and IR results and are simplified. Reproduced with permission from *Angew. Chem. Int. Ed.* **2009**, *48*, 9697-9700. Copyright (2009) Wiley-VCH.

Supported Metal Pair-Site Catalysts

The simplest supported catalysts beyond atomically dispersed single-site metal catalysts are those consisting of isolated pairs of metal sites. Such catalysts are considered prototypes for investigation of the role of neighboring metal centers in catalysis. Examples include rhodium pair sites on MgO and on SiO_2 investigated as catalysts for olefin hydrogenation[6-9] and ethylene hydroformylation.[10] Dinuclear iridium catalysts on α-Fe_2O_3 catalyze water photooxidation,[11] and catalysts inferred to incorporate pair sites of copper and of nickel in zeolites reportedly catalyze methane oxidation to methanol.[12, 13]

Synthesis
The most common strategy for synthesizing supported metal pair sites involves adsorption of a dinuclear organometallic precursor with metal–metal bonds intact and then activating

the supported species by modifying the remaining ligands. Examples of catalysts synthesized by this route include (a) rhodium pair-sites on MgO made from $Rh_2(\mu\text{-OMe})_2(COD)_2$ (OMe = methoxy; COD = cyclooctadiene) and from $Rh_2(OAc)_4$ (OAc = acetate); each of these precursors was adsorbed on the support from *n*-pentane solution.[6, 7]

Alternatively, rhodium pair sites on MgO have been made by a surface-mediated synthesis beginning with supported single-metal-site species, $Rh(C_2H_4)_2$/MgO, under conditions of mild hydrogenation, H_2 at 353 K.[8] We stress that this example of the simple formation of pair sites in the apparent absence of larger clusters is not likely to extend to other combinations of metals and supports, and it is not understood why it took place selectively in this example.

The dinuclear precursors typically react with support surface hydroxyl groups to form metal–support-oxygen bonds that anchor the metals. The choice of ligands is crucial. The

supported species are distinct from the precursors. Precursors typically have ligands that stabilize their dinuclear structures, such as bulky organic groups (e.g., substituted phosphines, bipyridine, or hydrocarbons).[14, 15] The organic ligands that remain on the anchored metal are typically inhibitors of catalytic reactions, and their removal can markedly increase the catalytic activity.

The removal and modification of ligands to increase the catalytic activities of supported metal species are exemplified the by mild hydrogenation of the species formed by adsorption of $Rh_2(\mu\text{-OMe})_2(COD)_2$ on MgO. The treatment replaces bridging methoxy ligands and forms methanol as well as hydride ligands that bridge the Rh centers; the COD ligands are hydrogenated to give cyclooctene, which remains on the support surface. Such treatments may not lead to structurally uniform supported species; more typically, there are changes in the nuclearity of the supported species.

In another synthesis method, a photochemical treatment was used to remove organic ligands from dinuclear iridium species on $\alpha\text{-Fe}_2O_3$ and form bridging oxo ligands, resulting in dimeric species that are active for water oxidation.[11]

Characterization and Structure

Metal pair-sites on supports have been characterized by (a) IR spectroscopy with CO as a probe ligand, with bridging carbonyl bands providing evidence of neighboring metal centers; (b) EXAFS spectroscopy indicating the number of near-neighbor metal atoms, on average; and (c) aberration-corrected scanning transmission electron microscopy (STEM) giving evidence of isolated metal pairs. The microscopy is effective only when there is a strong contrast between the supported metal atoms and the support (e.g. when heavy metal atoms are present on supports consisting of light atoms) and when sufficient images are obtained to give an accurate representation of the sample as a whole.

For illustration, Figure 4A is an IR spectrum of $Rh_2(\mu\text{-OMe})_2(COD)_2$ on high-area powder MgO and the sample after exposure to CO. Bridging CO bands at 1892 and 1849 cm^{-1} indicate Rh atoms in pairs.[6] We caution that not all supported rhodium pair-sites form bridging CO ligands when exposed to CO; for example, a sample made from $Rh_2(OAc)_4$ on MgO showed no bridging CO bands when exposed to gas-phase CO at room temperature, because the acetate ligands were not replaced by CO (Figure 4B). Instead, only one ν_{CO} band was observed, at 2117 cm^{-1}, representing a rhodium monocarbonyl species.[7]

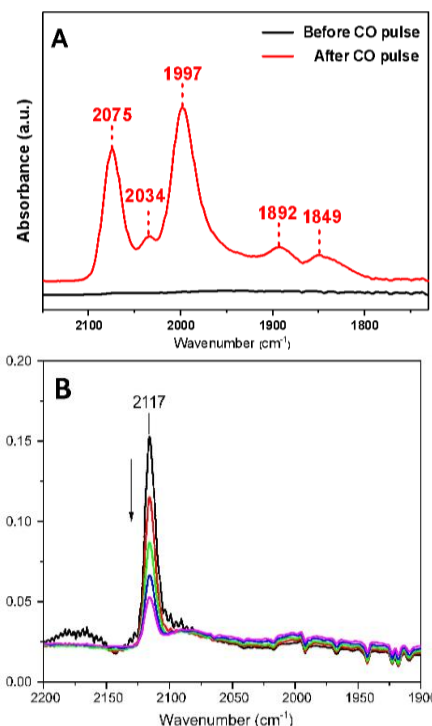Figure 4. IR spectra in the ν_{CO} regions characterizing the structures formed from (A) $Rh_2(\mu\text{-OMe})_2(COD)_2$ on MgO in helium and after exposure to flowing CO and (B) $Rh_2(OAc)_4$ on MgO formed by bringing CO in contact with the MgO-supported species formed from $Rh_2(OAc)_4$ for 2 min at 298 K, followed by treatment in flowing helium for 2 (black line), 4 (red), 6 (green), 8 (blue), and 10 min (pink). Reproduced with permission from *ACS Catal.*, **2018**, *8*, 482-487; *J. Catal.*, **2016**, *338*, 12-20. Copyright (2018) American Chemical Society and (2016) Elsevier.

EXAFS spectroscopy gives results showing average nuclearities of metal clusters, and a metal–metal coordination number of 1 is consistent with isolated metal pair-sites. The average metal–metal distance determined by EXAFS data can help to distinguish metals bonded to each other from those that are nearby but not bonded to each other. However, the distinctions are not always clear, for example, because the metal–metal distance may be influenced by the presence of bridging ligands. The Rh–Rh distance in a sample made from $Rh_2(OAc)_4$ on MgO is 2.39 Å, which is shorter than a Rh–Rh bonding distance in the MgO-supported rhodium dimer formed by treating supported $Rh(C_2H_4)_2$ in H_2 at 353 K for 1 h (2.71 Å), because the carboxylato-bridged $Rh_2(OAc)_4$ dimers imply multiple metal–metal bonds.[16] In contrast, the Rh–Rh distance in $Rh_2(\mu\text{-OMe})_2(COD)_2$ adsorbed on MgO is 2.83 Å, which is longer than a Rh–Rh single bond, indicating that the Rh atoms in the methoxy-bridged species are not bonded to each other.

The most direct way to demonstrate metal pair sites is to image them with atomic-resolution electron microscopy, typically high-angle annular dark field (HAADF) STEM. Figure 5, for example, is a STEM image showing the initial steps of metal aggregation from isolated $Ir(C_2H_4)_2$ species bonded to HY zeolite

in the presence of H_2 at 373 K. The heavy Ir atoms are observed as bright spots on the support. Another example (Figure 6) represents an α-Fe_2O_3-supported iridium pair-site catalyst.
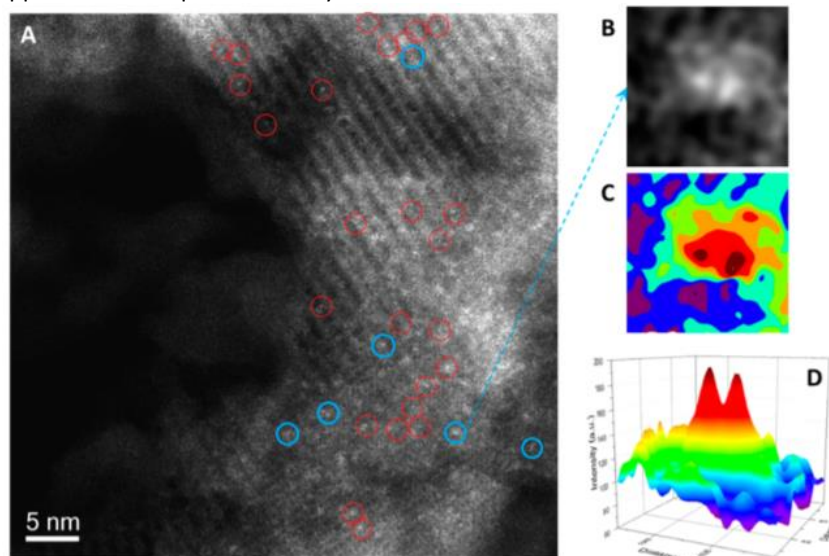

Figure 5. Aberration-corrected HAADF-STEM images characterizing $[Rh(C_2H_4)_2]^+$ complexes in zeolite Y, after treatment in flowing H_2 in helium at 373 K and 1 bar for 4 min, indicating the presence of supported Rh dimers (encircled in blue) along with single isolated Rh atoms (encircled in red). (B) A magnified view of the encircled area in (A) containing one Rh pair-site, with the intensity surface plot shown in (C) and the three-dimensional intensity surface plot shown in (D). Reproduced with permission from *J. Phys. Chem. Lett.*, **2016**, *7*, 2537-2543. Copyright (2016) American Chemical Society.
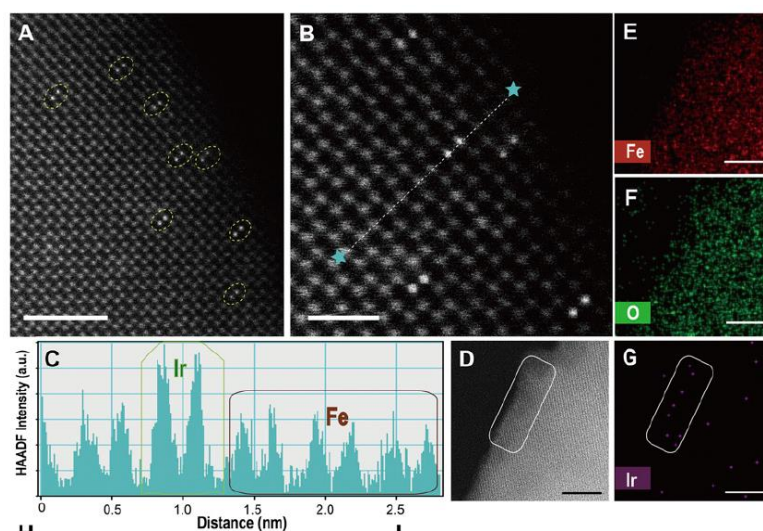

Figure 6. Images showing Fe atoms in α-Fe_2O_3-supported pair-site catalyst. A and B are representative HAADF-STEM micrographs along the [241] zone axis; the bright pairs are ascribed to iridium pairs. The dotted line between the two stars in B represents the line scan for the HAADF intensity analysis shown in C. (D) Dark field image of the region (outlined by white window) mapped in E–G for the distribution of Fe, O, and Ir, respectively. [Scale bars: (A) 2 nm; (B) 1 nm; (D–G): 4 nm.]. Reproduced with permission from *Proc. Natl. Acad. Sci.*, **2018**, 201722137. Copyright (2018) National Academy of Sciences of the United States of America.

The removal and modification of ligands on the supported metals is commonly characterized by IR and EXAFS spectroscopies. In the hydrogenation of Rh pairs synthesized from $Rh_2(\mu$-$OMe)_2(COD)_2$ on MgO, the formation of hydride ligands was indicated when the supported sample was exposed to a pulse of D_2, and product HD gas was detected in the effluent stream by mass spectrometry.[6]

Catalysis

Treatment in H_2 under mild conditions led to removal of bridging methoxy ligands and hydrogenation of cyclooctadiene ligands on Rh pair-sites synthesized from $Rh_2(\mu$-$OMe)_2(COD)_2$ on MgO. Correspondingly, during ethylene hydrogenation catalysis in a flow reactor, the activity increased with time on stream as these ligands were replaced by reactant ligands. The pair sites were found to be two orders of magnitude more active than

comparable single-site rhodium catalysts on MgO (Table 1), and it was inferred that the neighboring Rh centers facilitate more rapid H_2 dissociation and activation than the isolated Rh centers.[6]

Table 1. Rhodium single-site and pair-site catalysts supported on MgO: catalysts for ethylene hydrogenation. Modified from *ACS Catal.,* **2018***, 8,* 482-487. Copyright (2018) American Chemical Society

Model of Rh species initially present[a]	Ethylene hydrogenation activity, TOF (s^{-1})[b]
$Rh(CO)_2$/MgO	<0.0001
$Rh(C_2H_4)_2$/MgO	0.007
$Rh_2(\mu\text{-}H)_2(C_2H_5)_2$/MgO	0.038
$Rh_2(CO)_6$/MgO	<0.0001
$Rh_2(acetate)_3$/MgO	0.005
$Rh_2(\mu\text{-}H)_2(COE)_2$/MgO	1.1

[a]Predominant form of rhodium in catalyst, as determined by IR and EXAFS spectra. [b]Ethylene hydrogenation in a continuous plug-flow flow reactor at 298 K and 1 bar (feed H_2/C_2H_4 molar ratio, 1.0). The only catalytic reaction product was ethane. Turnover frequency (TOF) [(mol of ethylene converted) × (mol of rhodium × s)$^{-1}$] calculated from differential conversions by extrapolation to time on stream = 0.

Ligand modification can also improve catalyst selectivity. For example, Rh dimers on MgO are poisoned by CO, forming species approximated on the basis of IR spectroscopy as $Rh_2(CO)_6$/MgO.[9] This poisoned catalyst, once some of the CO ligands are removed, is active and highly selective for 1,3-butadiene hydrogenation to give *n*-butenes. The carbonyl ligands on the Rh dimers are essential, evidently limiting the activity for H_2 dissociation and favoring the partial hydrogenation of 1,3-butadiene. But the CO ligands are also reaction inhibitors, and as they were gradually removed from the catalyst during operation in a continuous flow reactor (Figure 7), the activity steadily increased. Yet the selectivity for *n*-butenes remained high until the CO coverage of the rhodium sites fell below a critical value, whereupon the selectivity plummeted (Figure 7). In contrast to the selectively poisoned pair-site catalyst, a comparable catalyst incorporating isolated single-site rhodium was active but unselective, and $Rh(CO)_2$ species were inactive. Attempts to make comparable species on other supports, such as γ-Al_2O_3, were not successful, indicating the importance of the MgO as a good electron-donor ligand.

Summary of opportunities and challenges

These results demonstrate the opportunities for tailoring catalytic properties by variation of the metal nuclearity, the ligands on the metal, and the support. The field of supported pair-site catalysts is in its infancy, and we might anticipate rapid advances and the discovery of catalysts in this class having new properties. A major challenge will

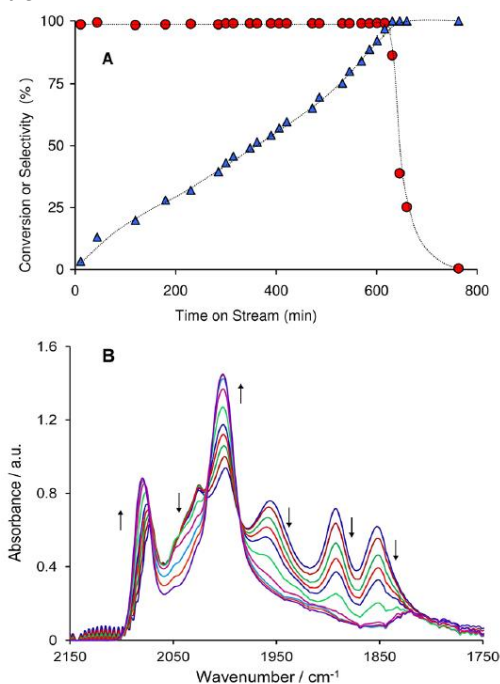be to synthesize new catalysts precisely and to find ways to make them stable.

Figure 7. (A) Change in conversion (▲) and selectivity (●) to *n*-butenes in 1,3- butadiene hydrogenation catalyzed by carbonylated rhodium pair sites supported on MgO in a once-through plug-flow reactor (reaction conditions: 313 K, 1 bar; total gas feed flow rate: 30 mL/min; feed component partial pressures, 20 mbar of C_4H_6, 980 mbar of H_2 ; mass of catalyst: 200 mg). (B) Time-resolved IR spectra of the MgO-supported rhodium carbonyl pair sites in a flowing mixture of 1,3-butadiene and H_2 at 313 K and 1 bar, showing that bridging CO ligands were removed preferentially, indicated by the downward-pointing arrows. Reproduced with permission from *ACS Catal.,* **2012***, 2,* 2100-2113*.* Copyright (2012) American Chemical Society.

Supported Metal Cluster Catalysts

In the following section, we consider metal clusters that have more than two metal atoms; many have polyhedral metal frames and typically incorporate ligands, which affect reactivity and help to stabilize the cluster frames. The clusters incorporate metal–metal bonds; the Rh–Rh bond distances in crystalline $Rh_6(CO)_{16}$ (which has an octahedral metal frame) and $Rh_4(CO)_{12}$ (which has a tetrahedral metal frame), for example, are 2.78 and 2.70 Å, respectively.[17, 18] Small as these clusters are, their physical and chemical properties are highly tunable by changing the cluster nuclearity, composition, and ligand environment.

We focus on structurally uniform supported metal clusters, containing less than 7 atoms, because these are small enough to yield informative structural data on the basis of EXAFS spectroscopy and STEM.

Synthesis

The most straightforward method of preparing supported metal clusters is to adsorb performed metal clusters on supports. Adsorption of metal clusters from the gas and liquid phases has led to many catalysts in this class, often retaining ligands that were present in the precursors, but not always retaining the compositions and structures of the precursors. We consider here examples for which characterizations by multiple techniques provide strong evidence of uniform clusters.

Various metal cluster compounds stabilized by small ligands, including $Ir_4(CO)_{12}$, $Rh_4(CO)_{12}$, $Rh_6(CO)_{16}$, $Os_3(CO)_{12}$, $Ru_3(CO)_{12}$, and so forth, or stabilized by chelating ligands, such as Pd_6L_4 (L denotes 1,3,5-tris(4-pyridyl)-2,4,6-triazine) and $Ir_4(CO)_9(L')_3$ (L' denotes a bulky calixarene-phosphine ligand) have been used as precursors of supported cluster catalysts.[5, 19-24]

The simple adsorption of precursors falls short as a preparation method when the supports (e.g., zeolites) have apertures too small to allow entry of the precursors. Then, ship-in-a-bottle syntheses are used, whereby a small adsorbed precursor (usually a mononuclear metal complex) is treated to form the clusters in place. For the preparation of uniform supported clusters, the cluster formation must take place with high yields. Examples are the synthesis of $Ir_6(CO)_{16}$ and $Rh_6(CO)_{16}$, from $Ir(CO)_2$ and $Rh(CO)_2$ complexes anchored to zeolite surfaces and formed, respectively, from the precursors $Ir(CO)_2(acac)$ and $Rh(CO)_2(acac)$ in zeolite NaY.[17, 25] These clusters are too large to fit through the zeolite apertures and remain trapped in the cages. Other examples and their structural parameters characterized by EXAFS data analysis are summarized in Table 2.

Structures

Structures of the metal frames of supported metal clusters have been determined by STEM images and by metal–metal coordination numbers and distances determined by EXAFS spectroscopy. Examples are shown in Table 2.

Table 2. EXAFS parameters characterizing various oxide-supported metal clusters.

Cluster	Support[a]	Precursor	EXAFS fitting parameters			Reference
			Shell	N	R (Å)	
$[Os_3(CO)_{11}]^{2-}$	MgO	$Os_3(CO)_{12}$[b]	Os–Os	2.1	2.89	24
			Os–C_{CO}	3.2	1.94	
			Os–O_{CO}	3.2	3.03	
			Os–O_{MgO}	1.0	2.16	
$Ir_4(CO)_{12}$	TiO2	$Ir_4(CO)_{12}$[b]	Ir–Ir	3.0	2.66	21
			Ir–C_{CO}	3.4	1.87	
			Ir–O_{CO}	3.0	3.02	
Ir_4 (stabilized by ethyl and di-σ-ethylene ligands)	HY zeolite	$Ir(C_2H_4)_2(acac)$[c]	Ir–Ir	3.0	2.68	26
			Ir–$O_{zeolite}$	1.3	2.11	
			Ir–C	2.07	6.4	
			Ir–Al	0.6	2.93	
$Ir_6(CO)_{16}$	NaY zeolite	$Ir(CO)_2(acac)$[c]	Ir–Ir_{1st}	4.0	2.74	25
			Ir–Ir_{2nd}	0.9	3.90	
			Ir–$O_{zeolite}$	0.8	2.11	
Ir_6	NaY zeolite	$Ir(CO)_2(acac)$[c]	Ir–C_{CO}	2.2	1.93	
			Ir–O_{CO}	2.2	3.00	
			Ir–Ir_{1st}	3.9	2.64	
			Ir–Ir_{2nd}	0.9	3.74	
			Ir–$O_{zeolite}$	1.3	2.09	

Notation: N, coordination number; R, distance between absorber and backscatter atoms. [a] The supports were treated under various conditions for partial dehydroxylation; details are provided in the references. [b] Supported metal clusters were prepared by direct deposition of the precursors onto oxide supports. [c] Supported metal clusters were prepared by ship-in-a-bottle synthesis, starting from smaller adsorbed precursors treated in reducing atmospheres. See the references for details.

Ligands present on the clusters have been characterized with spectroscopic methods, prominently with IR spectroscopy. NMR spectroscopy is also potentially valuable but has been applied far more to supported mononuclear species than to clusters.[27]

Ligands may be removed from supported clusters, but it is challenging to remove them while maintaining cluster nuclearity. Attempts to remove the ligands have usually been carried out at elevated temperatures or in reducing atmospheres, usually with changes in metal nuclearity (either cluster breakup or aggregation).[28] Several successful attempts have been made with clusters in confined environments, such

as zeolites, carbon nanotubes, or MOFs, which may stabilize the metal frames or limit migration of encapsulated species.

For example, Aydin *et al.* prepared $Ir_6(CO)_{16}$ in the pores of NaY zeolite by a ship-in-a-bottle synthesis, followed by removal of carbonyl ligands by treatment in flowing helium at 573 K.[25] EXAFS and HAADF-STEM data demonstrated that the metal frame of Ir_6 was maintained after the treatment. Other examples of cluster decarbonylation, such as of $Ir_4(CO)_{12}$ and $Rh_6(CO)_{16}$ in NaY zeolite, have also been reported.[17]

Supports may bond to clusters as ligands. Metal-support interactions can significantly influence cluster reactivity and stability. The interactions of clusters with supports are maximized when the cluster size is minimized. However, when the clusters become so large as metal nanoparticles, then the number of metal atoms interacting with the support becomes negligibly small and support effects become insignificant (unless complications such as support migration onto the metal ensue).

Evidence of the metal–support interface structure has been determined by EXAFS spectroscopy, which provides evidence of metal–support-oxygen bonds, with some results shown in Table 2. STEM images have also provided evidence of metal–support interfaces. For example, Kulkarni *et al.*[24] observed triosmium species on MgO (110) planes by HAADF-STEM. As illustrated in Figure 8, images showed that each Os atom in an Os_3 cluster was located atop an Mg atom and appeared in the image of the surface viewed from the top as the corners of an isosceles triangle. By considering the Mg–O–Mg–O ridges on the MgO (110) surface, the authors inferred two orientations of Os_3 bonded to that surface. Using the images in concert with DFT calculations, they demonstrated that the Os clusters interacted with the MgO by forming Os–O bonds at a distance of about 2.15 Å, with the Os_3 triangle tilted at an angle of 38° with respect to the MgO (110) surface.

The structures of various metal cluster precursors, including $Ir_4(CO)_{12}$, $Rh_4(CO)_{12}$, $Rh_6(CO)_{16}$ and $Os_3(CO)_{12}$ have been shown to remain intact and well-dispersed after adsorption on supports including MgO, SiO_2, γ-Al_2O_3, and TiO_2, as shown by spectroscopic and microscopic data. For example, Goellner *et al.*[21] prepared supported tetrairidium clusters by adsorbing $Ir_4(CO)_{12}$ on TiO_2. The ν_{CO} bands of the supported species nearly match those of $Ir_4(CO)_{12}$ in tetrahydrofuran solution. Complementary EXAFS data indicate an Ir–Ir shell with a coordination number of 3.0 ± 0.6, and each Ir atom was bonded to approximately three CO ligands. These results imply that the structure of $Ir_4(CO)_{12}$ was retained after adsorption.

On the other hand, metal cluster precursors react with some oxide surfaces in ways that change the ligand spheres of the metals. A number of examples illustrate metal carbonyl clusters adsorbed on basic metal oxides to form carbonylates; $[HIr_4(CO)_{11}]^-$ formed from $Ir_4(CO)_{12}$ on MgO, evidently as support hydroxyl groups reacted with the CO ligands bonded to Ir by nucleophilic attack.[29]
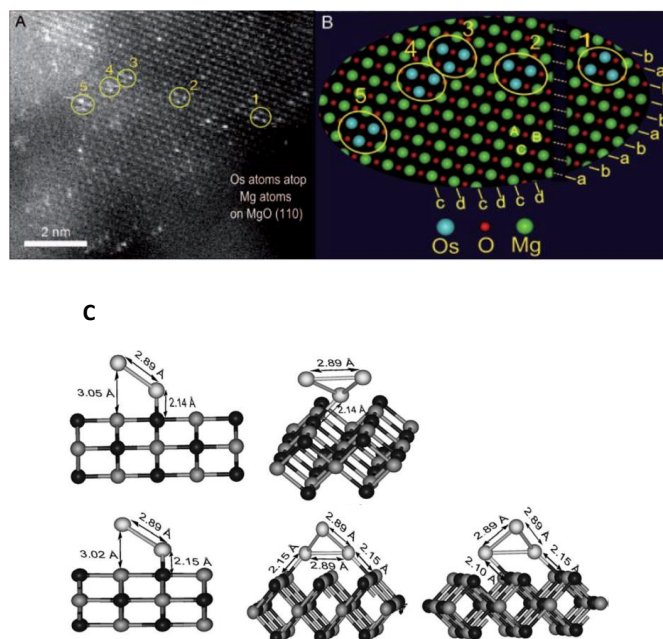

Figure 8. (A) Aberration-corrected STEM image showing individual Os atoms and Os atoms present in triosmium clusters whereby these atoms are positioned directly on top of Mg atoms on the MgO(110) surface. Circles denote intact supported triosmium clusters. The structure of the MgO(110) surface provided a calibration for determination of the Os–Os distances, as shown in the lower part (B). This represents a model of part of the image showing the positions of the Os atoms and models of the supported clusters. Reproduced with permission from *Angew. Chem. Int. Ed.* **2010**, *49*, 10089-10092. Copyright (2010) Wiley.

Among the few examples of cluster synthesis on supports that have been characterized in detail is one carried out as time-resolved IR and EXAFS spectroscopy experiments were used to track the process of cluster formation from supported $Ir(C_2H_4)_2$ in HY zeolite.[26] As the supported species reacted with H_2 acting as a reducing agent, EXAFS data (Figure. 9) were recorded showing that the Ir–Ir coordination number gradually increased and reached a maximum value of approximately 3, on average, indicating clusters with a tetrahedral metal frame. Concomitantly, the contribution of the Ir–O shell (O denotes the framework oxygen atoms of the zeolite) decreased, indicating breaking of Ir–O bonds; ethylene ligands bonded to the Ir centers were first converted into ethyl and di-σ-bonded ethylene ligands, then into ethylidyne and di-σ-bonded ethylene ligands, indicated by the IR results. The authors thus inferring the formation of tetrairidium clusters stabilized by hydrocarbon ligands and confined in the zeolite pores. Lu *et al.*[30] made similar observations under milder condition and inferring the formation of iridium hydride species that initiated the cluster formation.
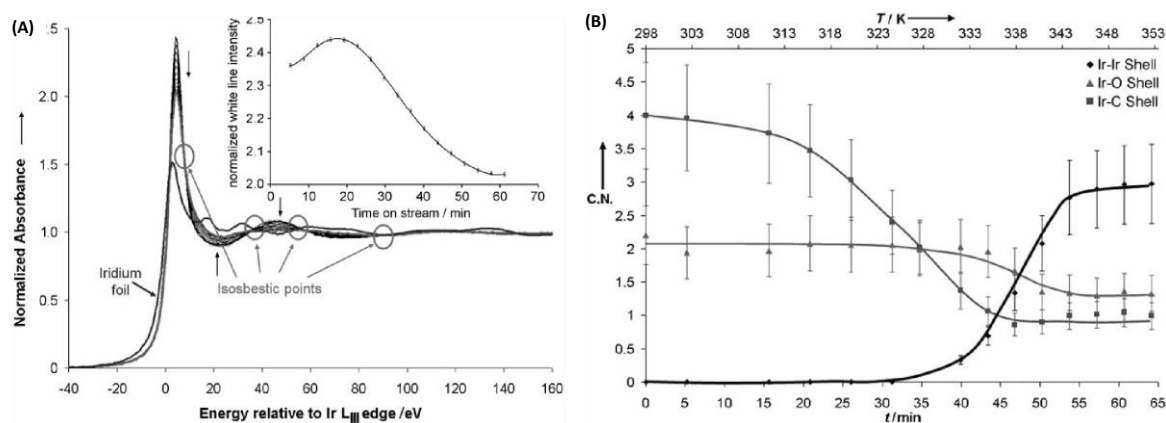
Figure 9. (A) Normalized XANES spectra at the Ir L$_{III}$ edge and (B) EXAFS data characterizing changes in the coordination numbers of the iridium in a sample formed from adsorbed Ir(C$_2$H$_4$)$_2$ on dealuminated Y zeolite during tetrairidium cluster formation as the temperature was ramped from 298 to 353 K (at 1 K min^{-1}) in flowing H$_2$ at 1 bar. Reproduced with permission from *Angew. Chem. Int. Ed.* **2008**, *47*, 9245-9248. Copyright (2008) Wiley.

It was further demonstrated that such changes in the nuclearity of the metal species could be observed during catalysis.[31] By carrying out *in operando* time-resolved EXAFS experiments to observe changes in the coordination numbers of the Ir–O and Ir–Ir shells, the authors observed that Ir(C$_2$H$_4$)$_2$ species in HY zeolite underwent cluster formation during catalytic ethylene hydrogenation when the feed was H$_2$-rich (C$_2$H$_4$/H$_2$ = 0.3). The average nuclearity of the resultant species in the steady state was nearly 4.0, mimicking the aforementioned situation in which the single-site Ir species were exposed to H$_2$. When the feed composition was switched to ethylene-rich (C$_2$H$_4$/H$_2$ = 4), the clusters were oxidatively fragmented to make single-site species. The reversible process is depicted schematically in Figure 10.

Similar observations were made for supported Rh(C$_2$H$_4$)$_2$ in HY zeolite, as shown in Figure 11, but the resultant clusters were not well defined and inferred to be present in a mixture.[32] The dynamic changes in the rhodium nuclearity led to changes in the catalytic selectivity in ethylene conversion: dimerization was dominant when the single-site rhodium was present, whereas hydrogenation prevailed as the nuclearity increased.
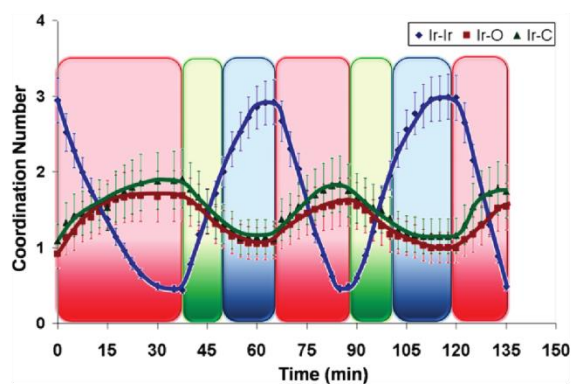
clusters approximated as Ir$_4$ to predominantly mononuclear iridium complexes followed a step-change in the feed to the flow reactor from H$_2$ to a mixture with a C$_2$H$_4$/H$_2$ = ratio of 4 (molar, indicated with a red background). After 35 min, the feed composition was switched to equimolar C$_2$H$_4$ + H$_2$ (green background). Then the feed ratio was switched to C$_2$H$_4$/H$_2$ = 0.3 (blue background). Subsequent changes are indicated by the color coding. The values of Δk (k: wave vector) and ΔR (R: distance) ranged from at least 4.0 to 12.5 Å^{-1} and from at least 1.2 to 3.2 Å, respectively. Reproduced with permission from *J. Am. Chem. Soc.* **2009**, *131*, 15887-15894. Copyright (2009) American Chemical Society.
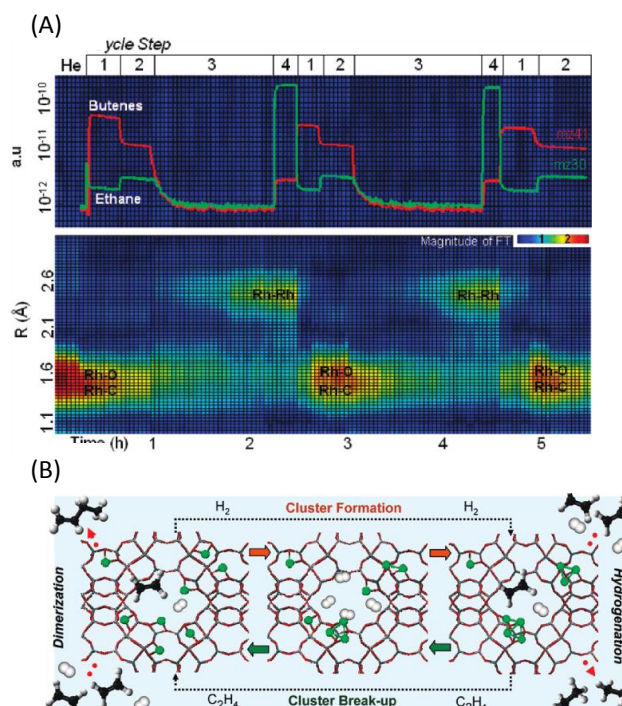

Figure 10. Changes in the EXAFS coordination numbers of functioning catalysts made from the precursor Ir(C$_2$H$_4$)$_2$(acac) and the support dealuminated HY zeolite. Conversion of

ARTICLE

Journal Name

Figure 11. (A) (top) Changes in selectivity of supported catalyst initially containing $Rh(C_2H_4)_2$ in HY zeolite and (bottom) structural changes represented by the Fourier transform of time-resolved EXAFS data as a function of the composition of the feed (shown as molar ratios), which was cycled in the following sequence: (1) 4:1:5 $C_2H_4/H_2/He$; (2) 1:4:5 $C_2H_4/H_2/He$; (3) pure H_2; (4) 1:4:5 $C_2H_4/H_2/He$. The experiment was carried out in a flow reactor that was an X-ray absorption spectroscopy cell at 303 K and 1 bar. In the bottom panel, the horizontal axis represents time on stream, the vertical axis the Rh–backscatterer distance (not corrected for phase shifts), and the colors the magnitudes of various contributions (related to the abundance of backscatterer atoms at a particular Rh–backscatterer distance. A change in color from red to yellow to green to blue shows a continuing decrease in intensity of the contribution).(B) Simplified representation of the state of the rhodium species (green) adsorbed in HY zeolite referred to EXAFS data analysis attained at each step in the cycle, as the catalytic performance changed with changes in the average rhodium nuclearity. Reproduced with permission from *J. Am. Chem. Soc.* **2011**, *133*, 4714-4717. Copyright (2011) American Chemical Society.

Catalysis

Small metal clusters may have substantial interactions with a support, with a significant fraction of the metal atoms bonded to it. These interactions affect reactivity. For example, Ir_4 on γ-Al_2O_3 that was prepared by decarbonylation of adsorbed $Ir_4(CO)_{12}$ was more than 10 times more active as a catalyst for propylene hydrogenation than the isostructural species on MgO.[33] The difference was explained by the different electron-donor strengths of the two supports, with MgO being the stronger electron donor. The more electron-deficient clusters on γ-Al_2O_3 were inferred to be the more active catalysts.

Besides metal oxides and zeolites, metal organic frameworks (MOFs) provide opportunities for anchoring of metal clusters. MOFs are porous crystalline materials consisting of inorganic nodes and organic linkers. The uniformity of MOFs commends them as catalysts incorporating well-defined species that can be understood fundamentally, and also as potentially selective catalysts. Such high selectivity is illustrated by the MOF-hosted linear Pd_4 clusters synthesized *in-situ* in the anionic network of the MOF $[Ni_4[Cu_2(Me_3mpba)_2]_3]^{4-}$ [Me_3mpba = N,N'-2,4,6-trimethyl-1,3-phenylenebis(oxamate)], which catalyze carbene-mediated reactions to make cycloheptatriene.[34] This reaction had previously been known to be catalyzed only by salts such as $Rh_2(OAc)_4$ in solution. The supported Pd_4 catalysts were found to be active and more selective (even shape selective, owing to the regularity of the MOF pores) and more stable than the rhodium salt. The work is unique in presenting a structure of a supported metal cluster determined by X-ray diffraction crystallography—a technique made possible because of the nearly uniform distribution of the Pd_4 clusters throughout the porous support.

These crystallographically precise materials open the way for the design of well-defined metal clusters and may lead to a large class of selective catalysts. But because MOFs are not perfectly crystalline materials, questions remain about the role of defects in determining reactivity and catalytic properties.

Single- or multiple-site catalysts

Extensive investigations of multinuclear catalysts demonstrate that neighboring atoms in small metal clusters work as multi-site catalysts that are comparable to metal surfaces. For example, investigations of olefin hydrogenation and aromatic hydrogenation catalyzed by Ir_4 and Ir_6 clusters supported on γ-Al_2O_3 and on MgO, involved measurements of reaction kinetics complemented with EXAFS, IR spectroscopy, leading Argo *et al.*[33, 35] to infer that hydride and hydrocarbon ligands were reaction intermediates and that the reaction mechanisms were comparable to those characteristic of iridium surfaces.

However, metal clusters can also act as single-site catalysts. Palermo *et al.*[22] demonstrated that the apical Ir sties on tetrairidium clusters supported on SiO_2, $Ir_4(CO)_9(L)_3$ (t-butyl-calix[4]arene(OPr)$_3$(OCH$_2$PPh$_2$)), protected by the bulky phosphine ligands, which are all bonded to Ir atoms in the basal plane, catalyze ethylene hydrogenation (Figure 12). The data show that the activity could be dialed in by plucking off CO ligands from the apical Ir atom and that the activity increased in direct proportion to the number of such opened sites. This work indicates opportunities to tune the activity at the apical site by choice of the ligands bonded to the basal plane sites.

Because metal clusters pose challenges for determination of structure and reaction mechanism, it is not generally straightforward to identify either single- or multi-site mechanisms of catalysis. Thus, the guidance of theory can be valuable, as illustrated for water oxidation catalyzed by ruthenium clusters embedded in polyoxometallate (POM).[36] DFT calculations indicated that a difference in minimum overpotentials of the single- and multi-site mechanisms in a catalytic cycle was only 0.16 eV and that the two mechanisms could even be occurring simultaneously.
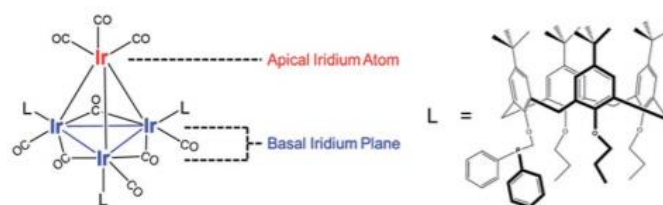
Figure 12. Schematic representation of a trisubstituted tetrairidium carbonyl cluster, closed cluster **1** ($Ir_4(CO)_9L_3$), with three bulky phosphine ligands on the basal plane of the tetrahedron (left); structure of calix[4]-arene phosphine ligand L shown at right. Reproduced with permission from *Chem. Sci.* **2017**, *8*, 4951-4960. Copyright (2017) The Royal Society of Chemistry.

Supported Metal Oxide Cluster Catalysts

Journal Name

ARTICLE

Metal oxide clusters have drawn much less attention than metal clusters as supported catalysts, primarily because it is challenging to synthesize them to be uniform. The most widely investigated metal-oxide-cluster catalysts are POMs.[37] Keggin-type POM clusters exemplified by $H_{8-n}X^{n+}W_{12}O_{40}$ (X = P, Si, Co, Al) are synthesized in acidic solutions; for example, $H_3PW_{12}O_{40}$ is formed by condensing phosphate ions with tungstate ions to give a heteropolyacid having the Keggin structure.[38] These clusters have been dispersed on supports exemplified by silica by incipient wetness impregnation. The resulting catalysts are active for acid-catalyzed reactions such as alcohol dehydrations, inferred to be catalyzed by Brønsted acid sites on the clusters. The number of these sites exposed on the supported Keggin clusters was determined by titration with pyridine during the catalytic reaction.[39, 40] The activities were found to be strongly dependent on the central atoms in the clusters, which determined the strengths of the Brønsted acid sites. The Keggin clusters maybe uniform in solution but become less than well-defined and often present in aggregates when they are on supports (with the nonuniformity associated with the synthesis method as well as the intrinsic nonuniformity of the support surface). The interactions between these clusters and the supports are not well understood.

A newer class of dispersed metal oxide cluster catalysts comprises MOFs that incorporate Zr_6O_8 and Hf_6O_8 clusters as the nodes. MOFs incorporating these nodes are UiO-66 (Figure 14a), UiO-67, NU-1000, and MOF-808. They offer the advantages of the structural uniformity of crystalline materials and dispersion in high-area solids, many of which have large enough pores for ready entry of reactant molecules and egress of product molecules. These MOFs have chemical and mechanical stability at high temperatures (up to 673 K), making them attractive in prospect as catalysts.

These MOFs are synthesized with liquid-phase reactants, whereby solutions containing metal salts and organic linkers are mixed together; alternatively a solvent is added to a mixture of a solid salt and a ligand in a reaction vessel.[41] For the synthesis of MOFs incorporating Zr_6O_8 nodes, modulators (e.g., formic acid, acetic acid, benzoic acid, or HCl) are added to facilitate the crystallization of MOF particles. The solvent dimethylformamide (DMF) plays important roles influencing MOF properties, and its decomposition product formate has been found to bond to the nodes, being the predominant ligand on them. [42] In the syntheses, modulators and/or ligands formed by decomposition of solvents compete with linkers in bonding to the initially formed metal oxide clusters, and they contribute to the formation of vacancies on the nodes. Work by Shearer et al. [43] demonstrated that both pK_a and the concentration of modulators added to synthesis mixtures may strongly affect the number of vacancies on the nodes.
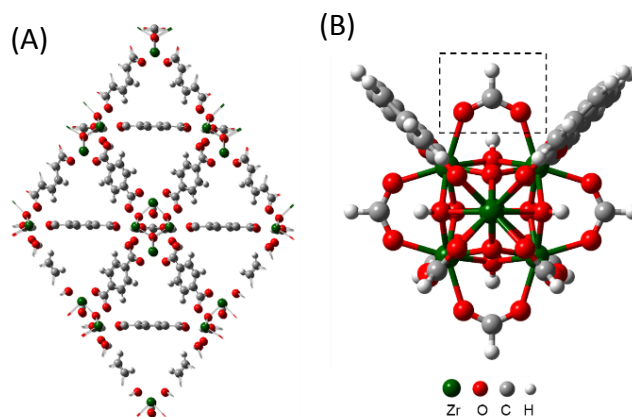

Figure 14. (A) Structure of UiO-66. (B) DFT-optimized formate-functionalized UiO-66 node. Note that the formate group at top (dashed box) is "unique" in being surrounded by benzoate groups that most accurately represent the linkers in UiO-66—the other formate groups depicted serve as truncated ligands for computational convenience. Reproduced with permission from *J. Am. Chem. Soc.* **2018**, *140*, 3751–3759. Copyright (2018) American Chemical Society.

The node chemistry is comparable to that of metal oxides, a widely applied class of catalysts. Thus, MOF nodes such as Zr_6O_8 clusters may be compared with zirconia, but they are significantly different, at least in part because they are small and uniform in structure.
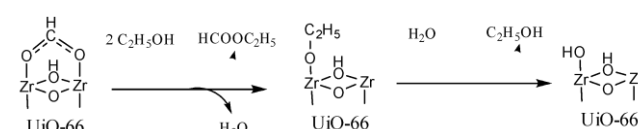
Scheme 1. Topology changes at missing linker sites of UiO-66 nodes. Reproduced with permission from *J. Am. Chem. Soc.* **2018**, *140*, 3751–3759. Copyright (2018) American Chemical Society.

Answers to some key questions about the catalytic nature of MOFs have been emerging only recently (Scheme 1),[42] because the ligands on the nodes have not been well characterized. Defects such as missing linkers in MOFs with metal oxide cluster nodes have been invoked to explain their adsorption and catalytic properties, and these act as the sites for bonding of ligands.

The compositions, reactivities, and catalytic properties of MOFs with Zr_6O_8 nodes have been investigated in experiments with probe molecules, including alcohols,[42] with ethanol dehydration being used as a catalytic test reaction because it occurs on metal oxide surfaces comparable to the Zr_6O_8 nodes and because both ethanol and the water formed as a product of the dehydration reaction react with these nodes.[42] The dehydration reaction catalyzed by the MOF nodes was found to be selective, with diethyl ether but not ethylene formed at 473–523 K. The clusters were also more active than the industrial catalyst γ-Al_2O_3. DFT calculations show that the key to the selective catalysis is the breaking of node-linker bonds (or the unintended presence of open sites (defects) on the nodes),

which allow catalytically fruitful bonding of the reactant ethanol to neighboring node sites, thereby facilitating the bimolecular ether formation via an S_N2 mechanism.

The stability of MOFs containing Zr_6O_8 nodes under catalytic ethanol dehydration conditions was found to depend strongly on the number of open (defect) sites on the nodes. As the number of these defects per node increased, the MOF became less stable, because ethanol reacted to break node-linker bonds and form esters with the linkers, thereby unzipping and destroying the MOF. At a relatively high temperature of 523 K, the unzipping was so fast UiO-66 was completely destroyed in only a few hours.[42]

The Zr_6O_8 nodes have also been found to be uniquely effective catalysts for the hydrolysis of the toxic nerve agent Sarin.[44] The vacancies on the MOF nodes have been inferred to act as Lewis acid sites, and the high activity of MOFs has been inferred to be the result of a high density of these sites. It was also reported that $-NH_2$ ligands on the organic linker dramatically accelerate the reaction.[45] DFT calculations demonstrated that these ligands control the microsolvation environment at the active site on the Zr_6-node and therefore increase the catalytic activity.[45]

To summarize, in contrast to supported POM clusters having less than well-defined structures on supports, the metal oxide clusters in MOFs are stabilized by strong coordination with organic linkers and are fully dispersed and have well-defined and more nearly uniform, essentially molecular structures than the supported Keggin ions. Isolated active sites on these metal oxide clusters are present in high densities and provide unique environments for catalysts that are potentially highly selective because they present nearly unique catalytic sites. The metal-oxide-cluster nodes in MOFs offer new opportunities for catalysis different from that on extended metal oxide surfaces, in part because the clusters are essentially molecular and limited in size and therefore may offer bonding opportunities different from those offered by the comparable metal oxides. The structural uniformity and molecular character of these nodes opens the way for catalyst design. Nonetheless, we emphasize that although MOFs are crystalline, they incorporate imperfections and less than uniform catalytic sites. And MOFs are limited in their potential applications as catalysts because of the limits of their stabilities at high temperatures and in some reactive environments, but we suggest that continuing discoveries of new MOFs and development of MOF with high stabilities may help them find catalytic applications.

Aggregation of Metal Nanoparticles

Supported metal nanoparticle catalysts typically undergo sintering of the metal under reductive conditions, and the corresponding loss of surface area often corresponds to significant activity loss. Researchers have attempted to minimize the sintering by encapsulating the nanoparticles in zeolite cages.[46] Such encapsulation hinders the aggregation, but usually does not prevent it. For example, Ir atoms present initially in isolated mononuclear complexes bonded in the straight parallel channels of the zeolite SSZ-53 as $Ir(C_2H_4)_2$ complexes were observed with STEM as the Ir atoms migrated

in the channels under the influence of the electron beam.[46] Initially, dimers formed, and then with continuing exposure to the beam, clusters too large to fit in the channels formed, and the crystalline zeolite structure was destroyed, as shown in Figure 15. Such sintering under reducing conditions had been known lead to the break-up of zeolite structures. It is clear that it would be advantageous to find a synthesis strategy to fix metal nanoparticles within a zeolite framework to prevent this collapse and loss of catalytic activity.
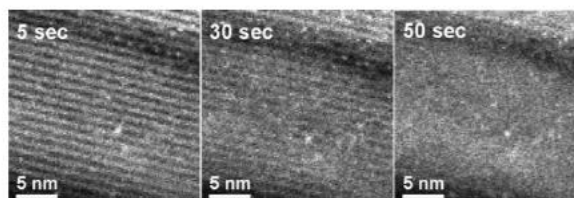

Figure 15. Effect of prolonged beam exposure on the zeolite framework. The crystalline structure of the zeolite was destroyed over time under the influence of the electron beam, leading to the loss of channel confinement of the migrating Ir atoms. Reproduced with permission from *Nano Lett.* **2011**, *11,* 5537–5541. Copyright (2011) American Chemical Society.

Stabilization of metal nanoparticles by zeolite encapsulation

Recent progress in the direction of stabilizing metal nanoparticles in zeolite matrices has been reported, with the advance linked to a novel synthesis method. The method provides stabilization of metal nanoparticles with diameters in the range of 1.5–4.0 nm, which is typical of industrial supported metal catalysts.

The new strategy for stabilizing metal nanoparticles in a zeolite matrix involves preparation of zeolite crystals from zeolite seed crystals that are pre-loaded with the metal nanoparticles. Strong interactions between these nanoparticles and the zeolite seed particles minimize the leaching and aggregation of the nanoparticles in the synthesis as zeolite crystals are formed and grow into a sheath around the zeolite particles that are the seeds, encapsulating them in a crystalline zeolite matrix.[47] Significantly, this sheath allows transport of reactant and product molecules without sintering of the metal nanoparticles. These encapsulated supported metal nanoparticles combine the advantages of the intrinsically high activities of the metal nanoparticles and the shape-selectivity attributed to the zeolite micropores. For example, when 4-nitrochlorobenzene is adsorbed on the catalyst consisting of palladium nanoparticles encapsulated in zeolite Beta, the reactant molecules align in parallel to the zeolite channels owing to the shape-selectivity, so that selective adsorption occurs with the nitro group rather than the chloro groups of 4-nitrochlorobenzene bonded to the Pd sites, consistent with the stronger bonding of nitro than chloro groups with these sites.[47] Thus, the zeolite-encapsulated palladium is selective for the hydrogenation of the nitro group rather than chloro group. In contrast, adsorption of 4-nitrochlorobenzene on a commercial Pd/C catalyst is best described as occurring with the aromatic ring interaction

parallel with the palladium surface, so that both the nitro and chloro groups interact with the Pd sites and are hydrogenated, and the catalysis is unselective.[47]

The encapsulation also confers excellent stability to these catalysts. In the typical supported noble metal nanoparticle catalyst, leaching and/or aggregation of the noble metal nanoparticles lead to deactivation. In contrast, metal nanoparticles confined within a zeolite sheath are stabilized. For example, in a long-term test of nitroarene hydrogenation catalysis, the zeolite-fixed palladium nanoparticles exhibited stable performances with undetectable aggregation or leaching of the palladium, whereas the conventional Pd/C catalyst was underwent rapid deactivation under the equivalent reaction conditions.[48] Even under harsh conditions, with catalytic reactions including the water-gas shift at 300 °C, CO oxidation at 200 °C, oxidative reforming of methane at 600 °C, and CO_2 hydrogenation at 350 °C, the zeolite-encapsulated catalysts were characterized by extraordinarily long lifetimes, outperforming the corresponding conventional supported metal catalysts and commercial supported metal catalysts.

Intrinsically Stable Iridium Nanoparticles

In the foregoing example, sinter-resistance was conferred by synthesis of the crystalline surroundings of the nanoparticles. But there is an example of a supported nanoparticle catalyst for which stability against sintering is an intrinsic property of the metal; the metal is iridium.

Iridium nanoclusters were prepared as follows, from single-site supported iridium complexes. Starting from the catalyst made by the reaction of $Ir(C_2H_4)_2(acac)$ with MgO, this single-site species was exposed to H_2 at 353 K and 1 bar for 1 h, leading to the formation of Ir_4 clusters in high yield, as described above. Further treatment of the supported Ir_4 clusters in H_2 at 673 K for 8 h led to the formation of iridium nanoclusters with diameters no larger than about one nanometer. Such intrinsic stability of nanoparticles is not known for metals other than iridium.

Conflicts of interest

There are no conflicts to declare.

Acknowledgements

Notes and references

1. B. C. Gates, M. Flytzani-Stephanopoulos, D. A. Dixon and A. Katz, *Catal. Sci. Technol.*, 2017, **7**, 4259-4275.
2. P. Serna and B. C. Gates, *Acct. Chem. Res.*, 2014, **47**, 2612-2620.
3. V. Aguilar-Guerrero, R. J. Lobo-Lapidus and B. C. Gates, *J. Phys. Chem. C*, 2009, **113**, 3259-3269.
4. J. Oliver-Meseguer, J. R. Cabrero-Antonino, I. Dominguez, A. Leyva-Perez and A. Corma, *Science*, 2012, **338**, 1452-1455.
5. A. Kulkarni and B. C. Gates, *Angew. Chem. Int. Ed.*, 2009, **48**, 9697-9700.
6. E. J. Guan and B. C. Gates, *Acs. Catal.*, 2018, **8**, 482-487.
7. D. Yang, P. H. Xu, E. J. Guan, N. D. Browning and B. C. Gates, *J. Catal.*, 2016, **338**, 12-20.
8. D. Yardimci, P. Serna and B. C. Gates, *Chem.-Eur. J.*, 2013, **19**, 1235-1245.
9. D. Yardimci, P. Serna and B. C. Gates, *ACS. Catal.*, 2012, **2**, 2100-2113.
10. K. Asakura, K. Kitamurabando, Y. Iwasawa, H. Arakawa and K. Isobe, *J. Am. Chem. Soc.*, 1990, **112**, 9096-9104.
11. Y. Zhao, K. R. Yang, Z. Wang, X. Yan, S. Cao, Y. Ye, Q. Dong, X. Zhang, J. E. Thorne and L. Jin, *Proc. Nat. Acad. Sci. USA*, 2018, 201722137.
12. J. J. Shan, W. X. Huang, L. Nguyen, Y. Yu, S. R. Zhang, Y. Y. Li, A. I. Frenkel and F. Tao, *Langmuir*, 2014, **30**, 8558-8569.
13. V. L. Sushkevich, D. Palagin, M. Ranocchiari and J. A. van Bokhoven, *Science*, 2017, **356**, 523-527.
14. B. Chaudret, B. Delavaux and R. Poilblanc, *Coord. Chem. Rev.*, 1988, **86**, 191-243.
15. U. Casellato and P. A. Vigato, *Chem. Soc. Rev.*, 1979, **8**, 199-220.
16. F. A. Cotton, B. G. Deboer, M. D. Laprade, J. R. Pipal and D. A. Ucko, *Acta Cryst. B-Struct.*, 1971, **B 27**, 1664-&.
17. W. A. Weber and B. C. Gates, *J. Phys. Chem. B*, 1997, **101**, 10423-10434.
18. L. J. Farrugia, *J. Clust. Sci.*, 2000, **11**, 39-53.
19. A. M. Argo and B. C. Gates, *J. Phys. Chem. B*, 2003, **107**, 5519-5528.
20. A. M. Argo, J. F. Odzak and B. C. Gates, *J. Am. Chem. Soc.*, 2003, **125**, 7107-7115.
21. J. F. Goellner, J. Guzman and B. C. Gates, *J. Phys. Chem. B*, 2002, **106**, 1229-1238.
22. A. Palermo, A. Solovyov, D. Ertler, A. Okrut, B. C. Gates and A. Katz, *Chem. Sci.*, 2017, **8**, 4951-4960.
23. P. Xin, J. Li, Y. Xiong, X. Wu, J. Dong, W. Chen, Y. Wang, L. Gu, J. Luo and H. Rong, *Angew. Chem. Int. Ed.*, 2018.
24. A. Kulkarni, M. F. Chi, V. Ortalan, N. D. Browning and B. C. Gates, *Angew. Chem. Int. Ed.*, 2010, **49**, 10089-10092.
25. C. Aydin, J. Lu, M. Shirai, N. D. Browning and B. C. Gates, *ACS. Catal.*, 2011, **1**, 1613-1620.
26. A. Uzun and B. C. Gates, *Angew. Chem. Int. Ed.*, 2008, **47**, 9245-9248.
27. J. D. A. Pelletier and J.-M. Basset, *Acct. Chem. Res.*, 2016, **49**, 664-677.
28. C. Aydin, A. Kulkarni, M. F. Chi, N. D. Browning and B. C. Gates, *J. Phys. Chem. Lett.*, 2012, **3**, 1865-1871.
29. S. Kawi and B. C. Gates, *Inorg. Chem.*, 1992, **31**, 2939-2947.
30. J. Lu, C. Aydin, N. D. Browning and B. C. Gates, *J. Am. Chem. Soc.*, 2012, **134**, 5022-5025.

31. A. Uzun and B. C. Gates, *J. Am. Chem. Soc.*, 2009, **131**, 15887-15894.
32. P. Serna and B. C. Gates, *J. Am. Chem. Soc.*, 2011, **133**, 4714-4717.
33. A. M. Argo, J. F. Odzak, F. S. Lai and B. C. Gates, *Nature*, 2002, **415**, 623-626.
34. F. R. Fortea-Perez, M. Mon, J. Ferrando-Soria, M. Boronat, A. Leyva-Perez, A. Corma, J. M. Herrera, D. Osadchii, J. Gascon, D. Armentano and E. Pardo, *Nat. Mater.*, 2017, **16**, 760-766.
35. A. M. Argo, J. F. Odzak, J. F. Goellner, F. S. Lai, F. S. Xiao and B. C. Gates, *J. Phys. Chem. B*, 2006, **110**, 1775-1786.
36. S. Piccinin, A. Sartorel, G. Aquilanti, A. Goldoni, M. Bonchio and S. Fabris, *Proc. Nat. Acad. Sci. USA*, 2013, **110**, 4917-4922.
37. X. Lopez, J. J. Carbo, C. Bo and J. M. Poblet, *Chem. Soc. Rev.*, 2012, **41**, 7537-7571.
38. Y. Izumi, K. Urabe and M. Onaka, *Zeolite, clay, and heteropoly acid in organic reactions*, VCH, 1992.
39. J. Macht, M. J. Janik, M. Neurock and E. Iglesia, *Angew. Chem. Int. Ed.*, 2007, **46**, 7864-7868.
40. J. Macht, M. J. Janik, M. Neurock and E. Iglesia, *J. Am. Chem. Soc.*, 2008, **130**, 10369-10379.
41. C. Dey, T. Kundu, B. P. Biswal, A. Mallick and R. Banerjee, *Acta Cryst. B*, 2014, **70**, 3-10.
42. D. Yang, M. A. Ortuño, V. Bernales, C. J. Cramer, L. Gagliardi and B. C. Gates, *J. Am. Chem. Soc.*, 2018.
43. G. C. Shearer, S. Chavan, S. Bordiga, S. Svelle, U. Olsbye and K. P. Lillerud, *Chem. Mater*, 2016, **28**, 3749-3761.
44. J. E. Mondloch, M. J. Katz, W. C. Isley III, P. Ghosh, P. Liao, W. Bury, G. W. Wagner, M. G. Hall, J. B. DeCoste and G. W. Peterson, *Nat. Mater.*, 2015, **14**, 512.
45. T. Islamoglu, M. A. Ortuño, E. Proussaloglou, A. J. Howarth, N. A. Vermeulen, A. Atilgan, A. M. Asiri, C. J. Cramer and O. K. Farha, *Angew. Chem. Int. Ed.*, 2018, **57**, 1949-1953.
46. C. Aydin, J. Lu, A. J. Liang, C. Y. Chen, N. D. Browning and B. C. Gates, *Nano Letters*, 2011, **11**, 5537-5541.
47. J. Zhang, L. Wang, Y. Shao, Y. Wang, B. C. Gates and F. S. Xiao, *Angew. Chem. Int. Ed.*, 2017, **56**, 9747-9751.
48. J. Zhang, L. Wang, B. Zhang, H. Zhao, U. Kolb, Y. Zhu, L. Liu, Y. Han, G. Wang, C. Wang, D. S. Su, B. C. Gates and F.-S. Xiao, to be published.